Accurate POD Reduced-Order Models of separated flows

J. Favier*, A. Kourta+ and L. Cordier†

* DICAT, via Montallegro 1, 16145 Genova, Italy
+ IMFT, Allée du Professeur Camille Soula, 31400, Toulouse, France
† LEA, UMR 6609 - CEAT, 43 route de l'aérodrome, 86036 Poitiers cedex, France
Julien.Favier@unige.it

Abstract

The objective of this work is to determine Reduced-Order Models based on Proper Orthogonal Decomposition (POD ROM) that can reproduce with a sufficient degree of reliability the spatio-temporal dynamics of separated flows. The growing interest for these models comes from their potential use as surrogate models in the resolution of large scale constrained optimization problems encountered in flow control. The general approach consists in substituting the high-fidelity model of Navier-Stokes equations by an approximate model, cheaper to compute and capturing the essential features of the original dynamics. POD, which is the optimal decomposition in terms of energy, can be used to describe the flow in a low dimensional subspace spanned by a few number of dominant modes. However, it can happen that the traditional POD-Galerkin approach leads to a POD ROM insufficiently accurate and even sometimes unstable. To improve the behavior of the POD ROM, various calibration methods are developed in this communication. Essentially, the idea of the calibration methods is to determine in the equations of the POD ROM auxiliary parameters that are computed by resolving appropriate constrained minimization problems. Finally, the calibration methods are assessed for two flow configurations of different complexity.

Keywords: POD Reduced-Order Models, calibration, optimization, flow control.

1. Introduction

Many attempts were already performed in order to suppress or to delay the boundary layer separation. A key enabler is the development of control procedures which are energetically efficient. To determine optimal control laws and thus to contribute to improve the current actuation systems, a method consists in formulating this flow control problem like a constrained optimization problem [8]. In practice, this problem of optimization is based on the minimization of an objective functional representative of separation (a functional of vorticity, for example). The objective of the optimal control theory is to determine control parameters (unsteady blowing/suction velocities) which minimize this cost functional under the constraints of the Navier-Stokes equations. The major difficulty comes from the iterative procedure of resolution generally used to solve this optimization problem which generates huge numerical costs when the Navier-Stokes equations are used as state equations. To circumvent this difficulty, reduced-order modeling is a powerful concept which allows a representation of the dynamics of large-scale systems by a small number of degrees of freedom (see Fig. 1), reducing considerably the numerical requirements associated to the optimal control approach.

Starting from a set of discretized state solutions, the idea of reduced-order modeling is to compress the information contained in the database in such a way to retain the essential features of the flow.

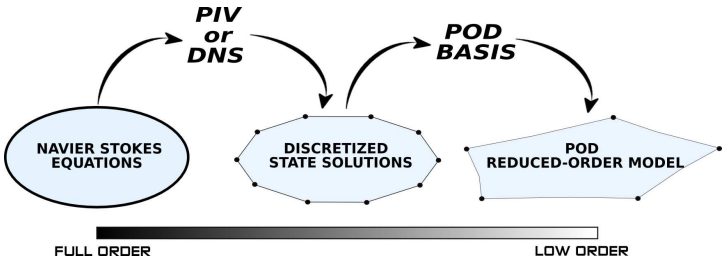

Figure 1. Schematic representation of the POD reduced-order modeling approach.

Using the Proper Orthogonal Decomposition (POD) [10, for example], it is possible to extract a set of modes characteristic of the database which constitute by construction the optimal basis for the energetic description of the flow. A Galerkin projection of the Navier-Stokes equations onto a finite number of POD modes yields a set of ordinary differential equations in time. The resolution of this POD Reduced-Order Model (POD ROM) provides a prediction of the temporal dynamics of the flow on the POD subspace. This model can then be used as surrogate model of the Navier-Stokes equations in an optimal control procedure. This approach was recently considered in [2] to control the wake flow of a circular cylinder in the supercritical regime.

With the aim of using these reduced-order models as surrogate models of Navier-Stokes equations, these POD ROM must be sufficiently accurate to reproduce the dynamics of the high-fidelity model. However, it is generally not the case for the POD ROM obtained directly by the traditional POD Galerkin approach. The main reasons are the truncation made in the POD subspace for the Galerkin projection, the intrinsic numerical instabilities of the model and the contribution of the pressure term which often should be modelled because the pressure is generally not accessible in the case of experimental data. To correct these approximation errors, calibration methods can be developed [4, 6]. Essentially, the aim of these calibration methods is to determine auxiliary parameters in the equations of the low-order model.

The general methodology of construction of a calibrated POD ROM is initially exposed in the case of a generic configuration of separated flow: the wake flow of a circular cylinder at $R_e = 200$ (DNS code Icare, IMFT). Then, this approach is assessed for a massively separated flow around a NACA012 airfoil at $R_e = 5000$ (DNS code Fluent). Thereafter, these two configurations are respectively called *DNS-cylinder* and *DNS-airfoil*.

2. POD-Galerkin modeling

Let $\left\{\mathbf{u}(\mathbf{x}, t_k)\right\}_{k=1,\ldots,N_t}$ be a set of N_t snapshots generated by DNS or PIV (velocity, pressure, temperature fields, $\ldots$) where $\mathbf{x} \in \Omega$ the physical space. Using the "method of snapshots" introduced by Sirovich [10], any snapshot can be expanded in terms of spatial POD eigenfunctions $\mathbf{\Phi}_i(\mathbf{x})$ and temporal POD eigenfunctions $a_i(t)$:

$$\mathbf{u}(\mathbf{x}, t) = \mathbf{u}_m(\mathbf{x}) + \sum_{i=1}^{N_t} a_i(t)\mathbf{\Phi}_i(\mathbf{x}), \tag{1}$$

where $\mathbf{u}_m(\mathbf{x})$ is the mean velocity estimated as an ensemble average of the flow realizations contained in the snapshot set. The energetic optimality of the POD basis suggests that only a very small number of POD modes $N_{gal} \ll N_t$ may be necessary to describe efficiently any flow realizations of the input data.

The weak form of the Navier-Stokes equations is then restricted to the POD subspace $\mathcal{E}_{N_{gal}}$

spanned by the first N_{gal} spatial eigenfunctions $\mathbf{\Phi}_i$. The Galerkin projection yields:

$$\left(\frac{\partial \mathbf{u}}{\partial t} + (\mathbf{u}.\vec{\nabla})\mathbf{u}, \mathbf{\Phi}_i\right)_\Omega = \left(-\vec{\nabla}p + \frac{1}{R_e}\Delta\mathbf{u}, \mathbf{\Phi}_i\right)_\Omega, \tag{2}$$

where $(.,.)_\Omega$ is the classical $\mathcal{L}^2$ inner product on Ω.

Finally, inserting the expansion (1) into the Galerkin projection (2), we obtain after some algebraic manipulations the following set of ODEs:

$$\begin{cases} \dot{a}_i(t) = \mathrm{C}_i + \mathrm{L}_{ij}a_j(t) + \mathrm{Q}_{ijk}a_j(t)a_k(t) + \left(-\vec{\nabla}p, \mathbf{\Phi}_i\right)_\Omega, \\ a_i(0) = \left(\mathbf{u}(\mathbf{x},0) - \mathbf{u}_m(\mathbf{x}), \mathbf{\Phi}_i(\mathbf{x})\right)_\Omega, \end{cases} \tag{3}$$

where the Einstein summation convention is used and all the subscripts run from 1 to N_{gal}.

The coefficients C_i, L_{ij} and Q_{ijk} depend explicitly on $\mathbf{\Phi}_i$ and $\mathbf{u}_m$. In the classical POD-Galerkin approach, these coefficients are first calculated once and for all at the beginning of the procedure. Then, the set of equations (3) is integrated in time with a fourth-order Runge-Kutta scheme yielding a set of predicted time histories for the mode amplitudes a_i, which can be compared with the POD temporal eigenfunctions $a_i^{\mathrm{ex}}(t_k) = (\mathbf{u}(\mathbf{x},t_k) - \mathbf{u}_m(\mathbf{x}), \mathbf{\Phi}_i(\mathbf{x}))_\Omega$ for $k = 1, \cdots, N_t$. For an incompressible flow, the pressure term writes $\left(-\vec{\nabla}p, \mathbf{\Phi}_i\right)_\Omega = -\int_\Gamma p\,\mathbf{\Phi}_i \cdot \mathbf{n}\, d\mathbf{x}$ where $\mathbf{n}$ is the outward unit normal at the boundary surface Γ. Here, we follow what is made in the majority of this type of studies [2, 6] and neglect at first approximation the contribution of the pressure term.

The dimension N_{gal} is determined in such a way that the major part of the flow energy is captured in the model. Figure 2 represents the relative energy contained in each POD mode for the cylinder configuration. This figure shows that for this flow configuration, the energy is concentrated in a very small number of modes: six POD modes are here sufficient to represent 99.9% of the flow energy. Thereafter, we thus consider $N_{gal} = 6$ for the *DNS-cylinder* configuration.

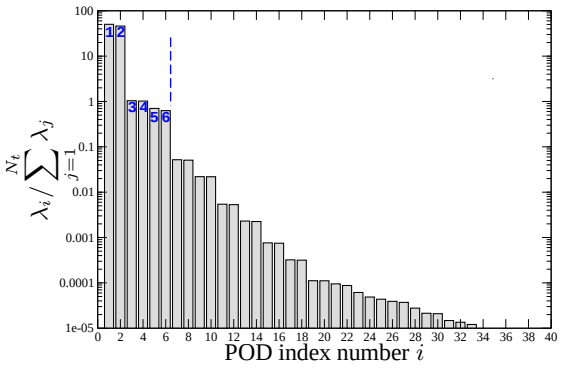

Figure 2. Relative energy content of the POD eigenvalue spectrum for the *DNS-cylinder* configuration. λ_i denotes the eigenvalue associated to the POD mode i.

When the POD ROM (3) is integrated in time under these conditions, the original flow dynamics is found globally but the precision is not perfect. As that is shown in figure 3, the most energetic mode is well reconstructed but for the higher modes, the maxima are over-estimated. This behavior is mainly due to the lack of dissipation generated by the truncation involved in the POD Galerkin approach. Indeed, the higher POD modes which correspond to the dissipative scales of the flow are not taken into account explicitly in the model. It is thus necessary to model their action, similarly as what is generally done in Large Eddy Simulation.

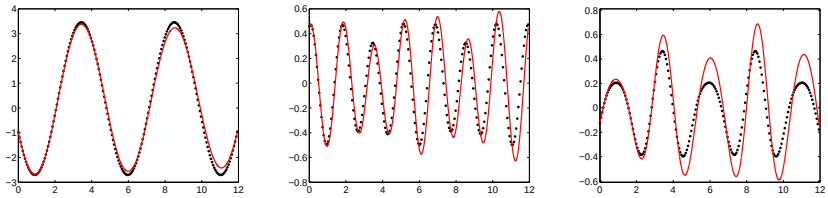

(a) $a_1(t)$ (b) $a_3(t)$ (c) $a_6(t)$

Figure 3. Comparison of the predicted (red lines) and reference (black symbols) mode amplitudes for the *DNS-cylinder* configuration. No calibration was used.

In the aim of improving the POD ROM predictive accuracy, various calibration methods are introduced in the following section where they are tested on the *DNS-cylinder* configuration. An application is then performed in section 4 on the *DNS-airfoil* configuration.

3. Calibration methods

Essentially, the idea of the calibration methods is to introduce into the POD ROM equations auxiliary parameters that are determined so that the amplitude coefficients $a_i(t)$, computed by solving (3), are as close as possible to the corresponding reference amplitudes $a_i^{\text{ex}}(t)$. A strategy consists in taking as a starting point the general philosophy of data assimilation methods [9]. We try to improve our knowledge of the system by combining as well as possible the observations of the system states (in our case the exact POD modes), and the form of the dynamical model (here obtained by the Galerkin projection). Consequently, these calibration terms can be estimated by considering two conditions of increasing level of constraint:

1. the form of the calibrated POD ROM equations has to fit the observations,
2. the temporal dynamics predicted by the calibrated POD ROM has to fit the observations.

3.1. Computing calibration terms

Following the analogy with Large Eddy Simulation in turbulence modeling, the calibration terms can be eddy-viscosities functions of the POD mode and eventually of time [1]. Another possibility is to add constant or/and linear terms to the set of equations [7, 3]. The number of free parameters in the calibrated system depends on the specific approach followed in the calibration procedure. In this study, the following calibration procedures are tested:

Cal. 1: linear terms G_{ij}: $\dot{a}_i(t) = \mathrm{C}_i + (\mathrm{L}_{ij} + G_{ij})a_j(t) + \mathrm{Q}_{ijk}a_j(t)a_k(t)$.

Cal. 2: constant terms F_i and linear terms G_{ij}: $\dot{a}_i(t) = (\mathrm{C}_i + F_i) + (\mathrm{L}_{ij} + G_{ij})a_j(t) + \mathrm{Q}_{ijk}a_j(t)a_k(t)$.

Cal. 3: eddy-viscosities α_i independent of time: $\dot{a}_i(t) = \mathrm{C'}_i + \mathrm{L'}_{ij}a_j(t) + \mathrm{Q}_{ijk}a_j(t)a_k(t)$ where $\mathrm{C'}_i$ and $\mathrm{L'}_{ij}$ are deduced from C_i and L_{ij} by adding an optimal correction factor $1 + \alpha_i$ to the term $1/R_e$.

3.2. Calibration using least squares procedure

To simplify the future description of the various calibration methods, let $\mathcal{C}_{ij}$ be the generic unknown calibration coefficients introduced in the previous section. Moreover, let us define $\hat{a}_i(t)$ the

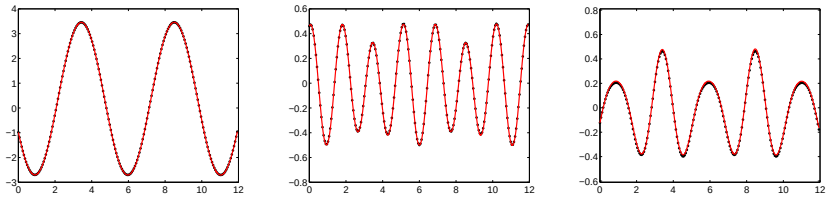

(a) $a_1(t)$ (b) $a_3(t)$ (c) $a_6(t)$

Figure 4. Comparison of the predicted (red lines) and reference (black symbols) mode amplitudes for the *DNS-cylinder* configuration. The reduced-order model obtained by Galerkin projection for $N_{gal} = 6$ was calibrated by addition of constant and linear terms.

continuous spline function that interpolates the set of points $\{(t_k, a_i^{\text{ex}}(t_k))\}_{k=1,\cdots,N_t}$. The calibration coefficients $\mathcal{C}_{ij}$ can be found as the solutions minimizing the following quadratic functional:

$$\mathcal{J}(\dot{a}_i, \mathcal{C}_{ij}) = \sum_{i=1}^{N_{gal}} \sum_{s=1}^{N_t} [\dot{a}_i(t_s) - \dot{\hat{a}}_i(t_s)]^2,$$

where the analytic expression of $\dot{a}_i(t)$ is given by (3) and $\dot{\hat{a}}_i(t)$ is estimated by numerically evaluating the time derivative of the reference spline.

The minimum of $\mathcal{J}$ is found when the partial derivatives $\partial\mathcal{J}/\partial\mathcal{C}_{ij}$ vanishe. This least squares problem gives rise analytically to a linear system that can be solved easily and rapidly to determine $\mathcal{C}_{ij}$. Indeed, the CPU time needed to compute the calibration terms is less than 0.5 second for the various calibration procedures considered. With this fast calibration procedure, we now obtain for the *DNS-cylinder* configuration an accurate POD ROM. This result is clearly highlighted on figure 4 where a calibrated model with constant and linear terms was used. The maxima overestimations which occur when the POD ROM is not calibrated are corrected. The prediction is now correct and even for high-order POD modes.

3.3. Comparison of different calibration procedures

In order to compare quantitatively the various calibration procedures introduced in section 3.1, we introduce $\mathcal{E}_i$, the temporal reconstruction error associated to the POD mode i, defined as:

$$\mathcal{E}_i = \frac{1}{N_t} \sqrt{\sum_{s=1}^{N_t} (a_i(t_s) - \hat{a}_i(t_s))^2}.$$

Figure 5 presents, for the *DNS-cylinder* configuration, the errors $\mathcal{E}_i$ obtained using the three calibration methods. Except for the first POD mode (see figure 5(a)) where the error is minimal when the POD ROM is calibrated by using a constant term, for the other POD modes the error is minimal when constant and linear terms are used for the calibration (for instance, figure 5(b) represents the error associated to mode 6). By adding the errors obtained for all POD modes, it appears that the calibration using constant and linear terms is the most efficient. In addition, for this flow configuration, the calibration using eddy viscosities constant in time provides a worse approximation than the other calibration procedures.

The differences between these calibration procedures can be explained by looking at the role played by the calibration coefficients on the model. In practice, the i^{th} constant term of calibration only alters the corresponding i^{th} POD mode dynamics, whereas the linear terms of calibration allow to exploit the interactions between modes i and j. Indeed, as one can note on figure 6, the

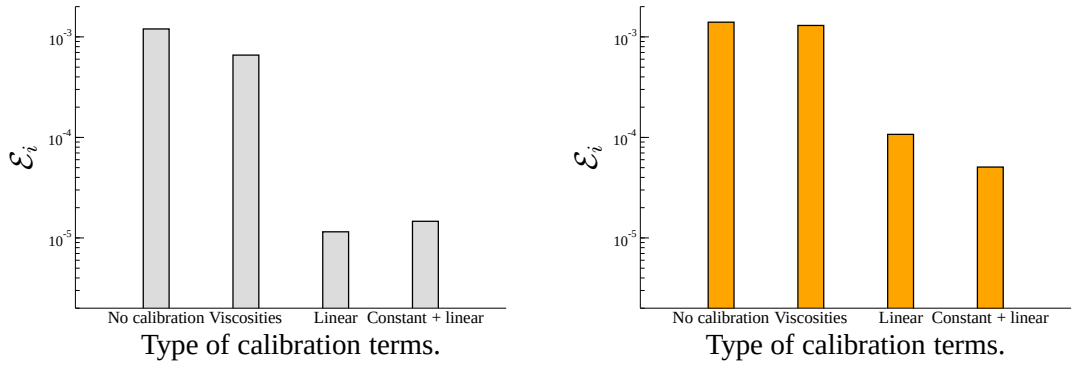

(a) Mode 1. (b) Mode 6.

Figure 5. Comparison for the *DNS-cylinder* configuration of the temporal reconstruction error $\mathcal{E}_i$ obtained for various kinds of calibration terms. Calibration is performed using the least squares procedure.

contributions of the linear calibration terms are greater for the off-diagonal terms, and it is all the more true for the higher POD modes. However, it is also noted that the interactions between modes are rather local. It seems that the corrections terms only alter the POD modes corresponding to the same scales. By nature, the calibration procedures based on the modification of eddy viscosities do not bring any possibility of interaction between POD modes. In that, their impact are similar to the calibration methods consisting in modifying the constant terms, even if in practice the constant and linear terms are corrected at the same time. To make this type of calibration more effective, it is interesting to consider time-dependent eddy viscosities [1]. The best relative efficiency of the calibration procedures based on the constant and linear terms seems to be explained by its impact on the whole model. Consequently, thereafter, the results concerning the calibration methods will be based on the determination of the constant and linear terms.

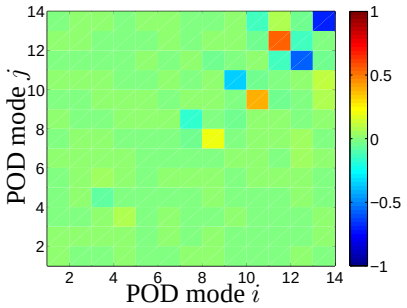

Figure 6. Graphical representation of the linear calibration term obtained for the *DNS-cylinder* configuration.

3.4. Constrained Optimization Procedure

Although the least squares procedure gives very good results in the case of the *DNS-cylinder* configuration, this approach only corresponds to the first condition stated at the beginning of section 3. A natural improvement of the previous approach consists in seeking the calibration terms as the solutions of a constrained optimization problem [8]. Indeed, one can consider that the calibration procedure is equivalent to determine *control parameters* (here, the constant and linear terms F_i and G_{ij}) which minimize the *cost functional* $\mathcal{J}$ (here, a measure of the difference between $a_i(t)$

obtained by the calibrated POD ROM and $\hat{a}_i(t)$ the coefficients of reference) given by:

$$\mathcal{J}(a_i, F_i, G_{ij}) = \sum_{i=1}^{N_{gal}} \sum_{s=1}^{N_t} \left[a_i(t_s) - \hat{a}_i(t_s)\right]^2,$$

under the constraints of the *state equations* (here, the calibrated POD ROM):

$$\dot{a}_i(t) = (\mathrm{A}_i + F_i) + (\mathrm{B}_{ij} + G_{ij})a_j(t) + \mathrm{C}_{ijk}a_j(t)a_k(t). \tag{4}$$

This constrained optimization problem is solved using the Lagrange multiplier method as described in [8]. The constraints are enforced by introducing the Lagrange multipliers or adjoint variables ξ_k, and the Lagrangian functional $\mathcal{L}$:

$$\mathcal{L}(a_i, F_i, G_{ij}, \xi_k) = \mathcal{J}(a_i, F_i, G_{ij}) - \sum_{k=1}^{N_{gal}} \sum_{s=1}^{N_t} \xi_k(t_s)\mathcal{N}_k(a_i, F_i, G_{ij}),$$

where the expression $\mathcal{N}_k(a_i, F_i, G_{ij}) = 0$ corresponds to the constraints (4).

Considering that each argument of $\mathcal{L}$ is independent of the others, the optimality system is determined by setting the first variation of $\mathcal{L}$ with respect to the adjoint variables ξ_k, the state variables a_i, and to the calibration terms F_i and G_{ij} to be equal to zero.

Setting the first variation of $\mathcal{L}$ with respect to the Lagrange multiplier ξ_k equal to zero, we recover the *state equation* $\mathcal{N}_k(a_i, F_i, G_{ij}) = 0$. When we set to zero the first variation of $\mathcal{L}$ with respect to the state variable a_i, the *adjoint equations* are derived. Finally, setting the first variation of $\mathcal{L}$ with respect to the control parameters F_i and G_{ij} equal to zero yields the *optimality conditions*. These equations are only equal to zero at the minimum of the objective function.

The *optimality system* formed by the state equations, the adjoint equations and the optimality equations represents the first order Karush-Kuhn-Tucker optimality conditions for the constrained optimization problem. This system of coupled ordinary differential equations is generally solved using an iterative method [see 1, for example] because the state equations associated to the optimization problem often correspond to a large-scale system (thousands or even million of degrees of freedom are frequently encountered in engineering computations). Here, it is possible to solve this system of coupled equations using a "one-shot" method because the state equations are formed by a low-order dynamical model with a very small number of modes. In this communication, we use the pseudo-spectral procedure recently suggested by [6]. The reader is referred to this article for a detailed description of the numerical procedure. The results obtained by the least squares approach can naturally be used to initialize the unknown control parameters and thus increase the speed of convergence of this procedure.

Figure 7 compares, for the *DNS-cylinder* configuration, the temporal reconstruction error $\mathcal{E}_i$ relative to the least squares calibration method to the one obtained with a constrained optimization method. For this benchmark configuration, the use of a more sophisticated optimization procedure improves the results obtained by the least squares approach, more particularly for the first POD modes *i.e.* the most energetic ones.

Finally, from a numerical point of view, the most efficient POD ROM calibration method, corresponds to the resolution of a constrained optimization problem. In addition to this aspect of pure numerical performance, this approach is also more satisfactory mathematically because it takes into account in a more complete way the constraints that the calibrated POD ROM must check. The next section thus applies this method to compute constant and linear calibration terms for the *DNS-airfoil* configuration.

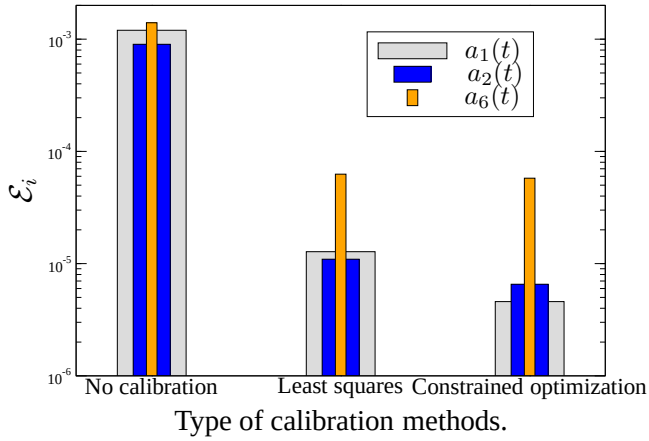

Figure 7. Comparison for the *DNS-cylinder* configuration of the temporal reconstruction error $\mathcal{E}_i$ obtained for various calibration methods.

4. Application to a massively separated flow around a NACA012 airfoil

In this section, we consider an incompressible two-dimensional vortex-shedding flow around a NACA012 airfoil, for a Reynolds number $R_e = 5000$ and an angle of attack $\alpha = 17^o$. The database was computed with the commercial code Fluent and is only composed of velocity snapshots. Figure 8(a) represents a typical snapshot contained in the database. The flow dynamics includes a vortex shedding at the leading edge, a massive separation on the upper-side of the airfoil, and a large wake downstream the trailing edge. As it can be inferred from Fig. 8(b), the energy of the flow is concentrated on the first POD modes, in a way similar to the first configuration.

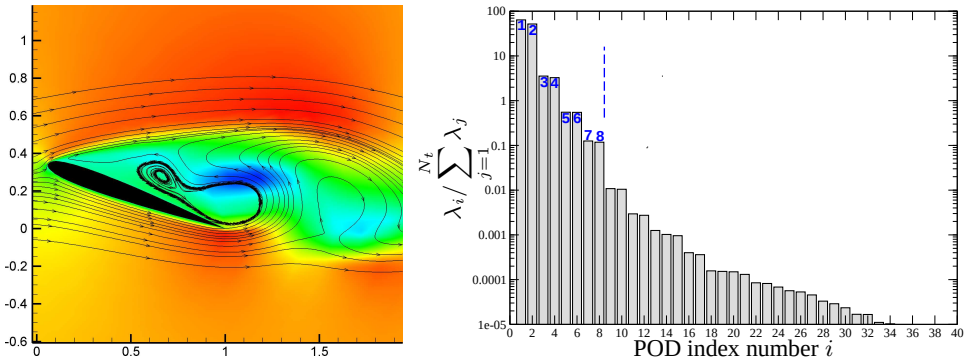

(a) Iso-values of the longitudinal velocity.

(b) Relative energy content.

Figure 8. One typical snapshot and relative energy content of the POD eigenvalue spectrum for the *DNS-airfoil* configuration.

The first 6 modes POD of the *DNS-airfoil* configuration are shown in Fig. 9. The spatial organization is close to that encountered classically in the literature for the *DNS-cylinder* configuration. Indeed, the POD modes are associated in pairs of same energy, which is characteristic of the strong periodic behavior of the Von Kármán vortex shedding in the wake of a cylinder. In the case of the *DNS-airfoil* configuration, the vortex shedding in the wake of the airfoil is also captured by POD, which allows a more efficient extraction of the dynamics of the coherent structures.

Following the same methodology as previously, a 8-modes POD-Galerkin system which also contains 99.9% of the flow energy is computed. The dynamics predicted by the POD ROM without

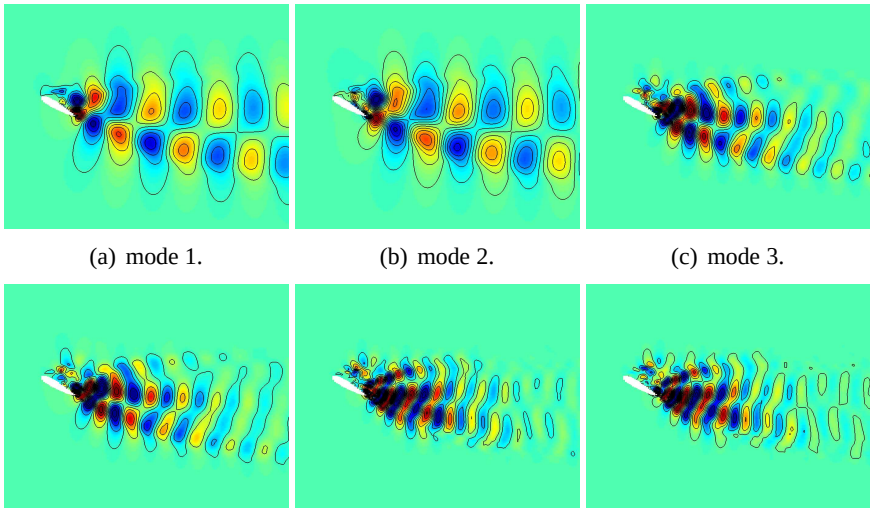

(a) mode 1. (b) mode 2. (c) mode 3.

(d) mode 4. (e) mode 5. (f) mode 6.

Figure 9. Iso-values of Φ_i^u longitudinal component of the spatial POD eigenfunctions $\mathbf{\Phi}_i$ for the *DNS-airfoil* configuration.

calibration is shown in Fig. 10(a). It appears that the temporal dynamics of the system is more unstable than in the case of the *DNS-cylinder* configuration. The maxima over-estimations are much more important than in the case of the *DNS-cylinder* configuration, in particular for higher POD modes where the model tends to diverge at long times.

At the opposite, the calibrated model using constant and linear terms computed as solutions of a constrained optimization problem presents a very good prediction of the system dynamics, even for the POD modes of high index. The over-estimates are corrected and we then succeed to have an accurate representation of the original dynamics.

5. Conclusion

For the two flow configurations tested in this study, accurate POD reduced-order models could be developed by using appropriate calibration procedures. The most efficient method appears to be the determination of constant and linear terms as solutions of a constrained optimization problem. In addition, in order to improve the speed of convergence of this procedure of optimization, let us mention that it is possible to use the control parameters obtained by the least squares method as initial values.

An immediate prospect of this work consists in solving a flow control problem via an optimal control approach by using a calibrated POD reduced-order model as state equations instead of Navier-Stokes equations. As the POD ROM generally depends on the design parameters used to derive it, it will be certainly necessary to use an adaptive technique of optimization in which the POD model is recomputed when the control parameters leave a zone called trust-region in which one estimates that the model is still representative of the controlled dynamics. Currently, the most suitable method is the TRPOD algorithm recently proposed in [5]. This approach should allow in a near future to tackle realistic flow control problems.

References

[1] M. Bergmann. *Optimisation aérodynamique par réduction de modèle POD et contrôle optimal. Application au sillage laminaire d'un cylindre circulaire.* Thèse de doctorat, Institut

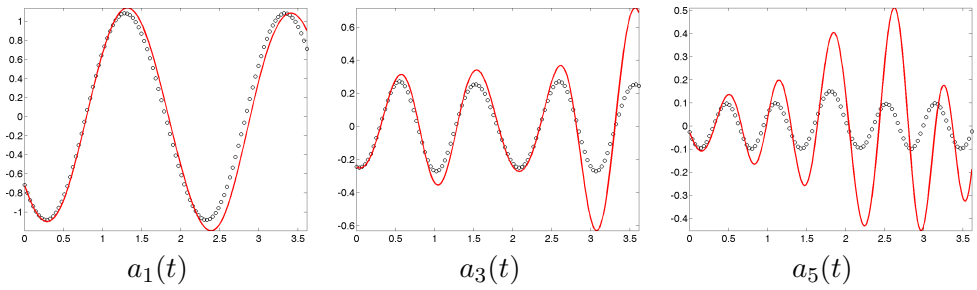

(a) Uncalibrated ROM.

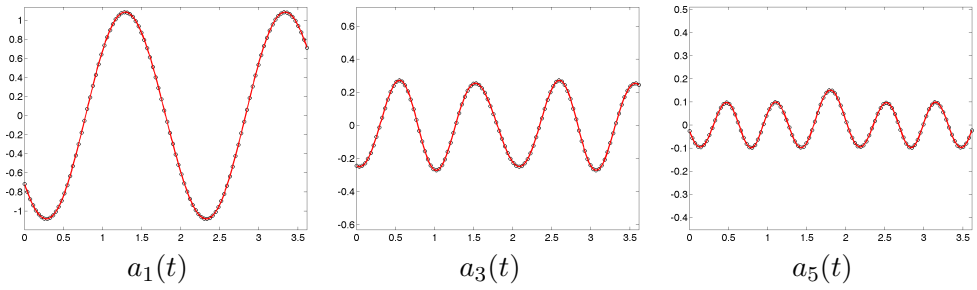

(b) Calibrated ROM.

Figure 10. Comparison of the predicted (red lines) and projected (black symbols) mode amplitudes for the *DNS-airfoil* configuration. The reduced-order model obtained by Galerkin projection for $N_{gal} = 8$ is used without and with calibration of the coefficients.

National Polytechnique de Lorraine, Nancy, France, 2004.

[2] M. Bergmann, L. Cordier, and J.-P. Brancher. Optimal rotary control of the cylinder wake using POD Reduced Order Model. *Phys. Fluids*, 17(9):097101:1–21, 2005.

[3] M. Buffoni, S. Camarri, A. Iollo, and M.V. Salvetti. Low-dimensional modelling of a confined three-dimensional wake flow. *J. Fluid Mech.*, 569:141–150, 2006.

[4] M. Couplet, C. Basdevant, and P. Sagaut. Calibrated Reduced-Order POD-Galerkin system for fluid flow modelling. *J. Comp. Phys.*, 207:192–220, 2005.

[5] M. Fahl. *Trust-Region methods for flow control based on Reduced Order Modeling*. Thèse de doctorat, université de Trier, 2000.

[6] B. Galletti, A. Bottaro, Bruneau C.-H., and A. Iollo. Accurate model reduction of transient flows. Technical Report 5676, INRIA, 2005.

[7] B. Galletti, C.-H. Bruneau, L. Zannetti, and A. Iollo. Low-order modelling of laminar flow regimes past a confined square cylinder. *J. Fluid Mech.*, 503:161–170, 2004.

[8] M. D. Gunzburger. Introduction into mathematical aspects of flow control and optimization. In *Lecture series 1997-05 on inverse design and optimization methods*. Von Kármán Institute for Fluid Dynamics, 1997.

[9] E. Kalnay. *Atmospheric Modeling, Data Assimilation and Predictability*. Cambridge University Press, 2003.

[10] L. Sirovich. Turbulence and the dynamics of coherent structures. *Quarterly of Applied Mathematics*, XLV(3):561–590, 1987.